Atomic Force Microscopy

Piontek, Melissa C; Roos, Wouter H

Published in:
Methods in Molecular Biology

DOI:
10.1007/978-1-4939-7271-5_13

Publication date:
2017

Chapter 13

Atomic Force Microscopy: An Introduction

Melissa C. Piontek and Wouter H. Roos

Abstract

Imaging of nano-sized particles and sample features is crucial in a variety of research fields. For instance in biological sciences, where it is paramount to investigate structures at the single particle level. Often two-dimensional images are not sufficient and further information such as topography and mechanical properties are required. Furthermore, to increase the biological relevance, it is desired to perform the imaging in close to physiological environments. Atomic force microscopy (AFM) meets these demands in an all-in-one instrument. It provides high-resolution images including surface height information leading to three-dimensional information on sample morphology. AFM can be operated both in air and in buffer solutions. Moreover, it has the capacity to determine protein and membrane material properties via the force spectroscopy mode. Here we discuss the principles of AFM operation and provide examples of how biomolecules can be studied. By including new approaches such as high-speed AFM (HS-AFM) we show how AFM can be used to study a variety of static and dynamic single biomolecules and biomolecular assemblies.

Key words Atomic force microscope (AFM), High-speed AFM, Topography, Force spectroscopy, Cantilever, Contact mode, Intermittent contact mode, Biological applications, Nano-indentation

1 Introduction

While performing research at the cellular and subcellular level, suitable imaging tools are essential to come to an in-depth description of the processes that occur at these length scales. A variety of instruments has been developed to study biology at the micro- to nanoscale. A landmark invention was the light microscope, which uses photons interacting with the sample surface and lenses to create a magnified image of the specimen. At the end of the seventeenth century, Antonie van Leeuwenhoek made this technique popular under biologists. Significant development of this technique occurs up to date. In the early 1930s E. Ruska and M. Knoll invented another instrument making a specimen and its surface visible: the Electron Microscope (EM). Here, electrons instead of photons function as probes to create an image of the sample surface. Images acquired with EM have a significantly higher

Erwin J.G. Peterman (ed.), *Single Molecule Analysis: Methods and Protocols*, Methods in Molecular Biology, vol. 1665, DOI 10.1007/978-1-4939-7271-5_13,

resolution than the ones obtained with the optical microscope. For both approaches the resolution is basically being limited by the used wavelength, which is much smaller in the case of EM [1]. Still, the corresponding data does not provide quantitative height information and, consequently, is two-dimensional.

Successful experiments providing three-dimensional information at the nanoscale were conducted using Scanning Tunneling Microscopy (STM). They were first presented by Binnig and Rohrer in 1982 [2]. The technique uses a metal tip mounted at the end of a cantilever. The tip is approached to the surface and scans the surface while the tunnel current is kept constant with a feedback control. The voltage applied to the piezo-drivers is used to move the tip in the z-direction, keeping the tunnel current constant, and to move the tip in the x- and y-direction to scan the surface. Hereby the topography of the sample's surface is being reconstructed. Since the tunnel current is extremely sensitive to alteration of the distance (exponential dependence), atomic resolution is achievable [1, 2]. Drawback of this technique is the need for conductive samples and probes. For instance, biological samples are insulators and thus it is impossible to image them with this approach. Coating of the sample with a conducting layer can solve this problem, however, thereby making the substrate less relevant for biological experiments.

With the advent of the Atomic Force Microscope (AFM) by Binnig *et al.* in 1986 [3], not only the limitations of the resolution of optical microscopes were overcome, but also the requirements of the sample being conductive. Instead of using the tunneling current, an AFM takes advantage of the interacting force between the tip and the surface, which deflects the cantilever. In combination with a feedback control, the topography of the sample surface can be reconstructed [4, 5]. The big advantage of this approach is that any sample can be investigated, because there is no need for conductivity. This invention facilitates great possibilities especially in biological sciences as proteins, viruses, cells, and membranes can be imaged at nanometer resolution [1, 6–10].

The principle of AFM is also applicable for magnetic samples. The corresponding measurement instrument is called Magnetic Force Microscopy (MFM). The main difference between an AFM and a MFM is the tip itself. In an AFM it is nonmagnetic, while the tip of a cantilever inserted in a MFM is made of ferromagnetic material. In MFM the magnetic field gradient causes a force acting on the tip which bends the cantilever and imaging is performed by measuring the interaction between the tip and this magnetic field. The range in which a high spatial resolution can be obtained is 10 nm–100 nm [11].

With all of the aforementioned devices, that provide more than two-dimensional information, a new level of data acquisition has become possible. STM, AFM and MFM all belong to the group

called "Scanning probe microscopes," which in a way can be regarded as a combination of the techniques of profilers and SEM [5]. The invention of the electron microscope and the STM was awarded with the 1986 Nobel Prize in Physics. E. Ruska, G. Binnig, and H. Rohrer received the prize, the former for his work on EM and the latter two for their work on the STM.

Besides nanometer spatial resolution, many researchers were also looking for instruments reporting information on the fourth dimension, i.e. high temporal resolution. While for traditional AFM it typically takes several minutes to record one image, the endeavor was to reach sub-second temporal resolution. Several approaches to develop so-called high-speed AFM (HS-AFM) have been undertaken [12]. The approach of T. Ando has turned out to be the most practical for observing biomolecular processes and imaging rates of >10 frames per second are now routinely possible [13, 14]. Using HS-AFM the observation of real-time dynamic processes in liquid is possible and therefore, has a great potential in biological sciences [15].

2 Basics of AFM

This section discusses the basics of the AFM technique, the set-up as well as various operation modes.

2.1 Set-Up and Principle

AFM image acquisition is based on attractive and repulsive interactions with the sample. The set-ups typically consist of, among others, the following components [5, 16]:

- A cantilever, which has a sharp tip at its end.
- A detection system of the cantilever's bending.
- A feedback control of the applied force and the distance.
- A movement system (e.g. piezo tubes) to enable the scanning of the sample surface in all three dimensions with respect to the cantilever.
- A graphical visualization system of the acquired data.

A simplified schematic illustration of an AFM is shown in Fig. 1a and an example image of a virus acquired with an AFM is presented in Fig. 1b.

The so-called optical beam deflection (OBD) method is a common method to detect topography changes by AFM [18]. For the measurement of the bending of the cantilever, a laser beam is focused on the rear side of the cantilever. The rear side itself can be coated to enhance the amount of the reflected laser light, but this coating is not always necessary and it should be kept in mind that this coating could affect the thermal stability [19]. In either case, with or without coating, the reflected light will be

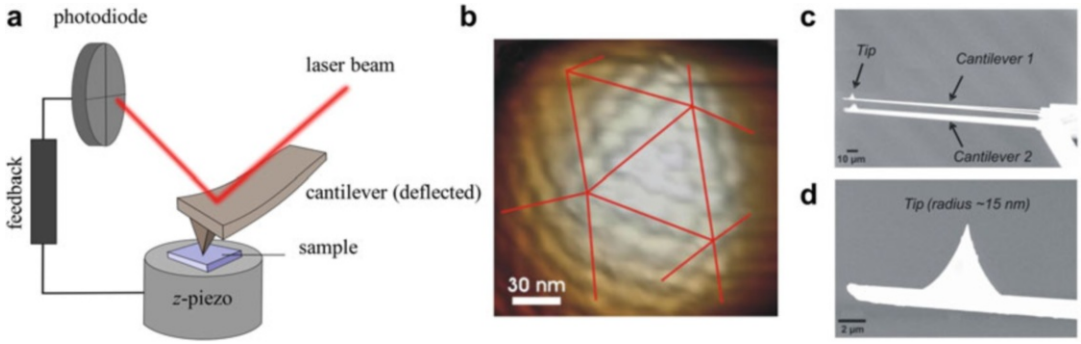

Fig. 1 AFM set-up. (**a**) This schematic represents a so-called sample-scanning configuration. An alternative is a system where the cantilever is scanned, i.e. a tip-scanning configuration. Combinations using linear piezos are also possible. (**b**) Example image of AFM. This picture of a virus, imaged in buffer solution, shows how AFM imaging can reveal structural features of biological substrates such as in this case protein clusters and icosahedral facets. Reproduced from ref. 17 with permission from PNAS. (**c**) Cantilever electron microscopy image. Two cantilevers with different spring constants are attached to the chip. Cantilever 1 is in focus, cantilever 2 is out of focus. (**d**) Zooming in onto the tip reveals that it is not infinitely sharp, but actually has a radius of curvature of approximately 15 nm.

directed to a quadrant photodiode, which detects positional alterations in the reflected light. Whenever the interaction force between the tip and the sample surface changes, the cantilever will bend, and thus the position of the laser spot on the photodiode changes. The measured signals are transmitted to the feedback electronics, processed and converted into a voltage which is used to retract or extend the piezo. Dependent on the actual AFM configuration, the movement of the piezo is used either to change the position of the sample or the cantilever. These are the two different ways to scan the sample surface. One possibility is that the position of the cantilever is fixed while the sample is moved by the piezoelectric element. Alternatively, the sample is fixed and the cantilever including the OBD-system is translated. The maximum scan range for x and y is on the order of ~100 µm times ~100 µm, while in z-direction this is ~30 µm. However, systems with larger scan ranges are also being used and many systems have (much) smaller scan ranges.

The cantilevers are typically fabricated from silicon or silicon nitride. To ensure operation in a variety of different AFM instruments, the dimensions of the cantilever base are industrially standardized. The base (chip) of cantilevers is usually about 3.5 mm long, 1.6 mm wide and it has a thickness of 0.5 mm. The typical length for rectangular cantilevers is ~200 µm–400 µm with a width of ~20 µm–40 µm [5]. Next to rectangular cantilevers also triangularly shaped ones are common, which are also called "V-shaped". The tip radius is typically ~15 nm–20 nm, but oxide sharpened tips with smaller radii are also available. Figure 1c, d show electron micrographs of example cantilever and tip. Besides the tip radius,

the cantilever spring constant k is also a characteristic quantity. It is dependent on the dimensions of the cantilever and the Young's modulus of the used material. Next to the often used vertical spring constant, also the lateral and torsional spring constant can be of importance. Typical values for the vertical spring constant range from a bit below 0.1 N/m to higher than 10 N/m [5]. While the manufacturer provides the specifications of their product, it is recommended to calibrate the cantilever spring constant before each measurement [20].

2.1.1 Tip Sample Interactions

The dimension of the tip strongly affects the resolution of the acquired topography. Because the tip dimension is finite, the resulting image is always a convolution of the tip and the sample. Figure 2 shows three possible imaging scenarios. In case the tip is small compared to the sample, an image which represents mostly the sample is acquired (Fig. 2a). Figure 2b shows a situation where the tip radius and sample size are roughly equal to each other, resulting in an image representing features from both tip and sample. In contrast, images acquired with a tip which is much larger than the sample, predominantly reflect the tip geometry itself (Fig. 2c).

The tip size can be reconstructed using an array of spikes. One of such spikes is shown in Fig. 2c. Furthermore, the tip size and geometry can be altered. For instance, it is possible to use controlled wear of the tip to create a defined spherical tip shape with increased radius. Corresponding experiments and results were recently reported by Vorselen *et al.* [21]. Here, high roughness polycrystalline titanium and ultrananocrystalline diamond surfaces were used to map the tip dimension. This mapping was performed at low imaging forces. Furthermore, by increasing the imaging force, the authors were able to dynamically increase the tip radius and to monitor this increase in real-time. While typical wear experiments result in blunted tips, in this approach spherical tips with the

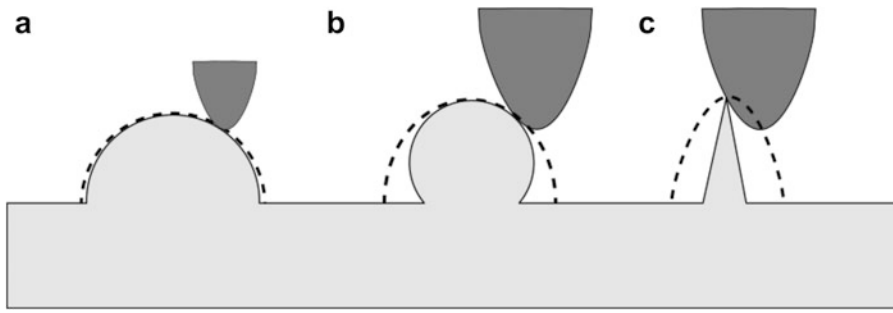

Fig. 2 Tip geometry affects the data in AFM imaging. The *dashed lines* represent the measured height profile. (**a**) The tip size is much smaller than the sample; (**b**) sample and tip dimensions are comparable; and (**c**) the tip is much larger than the sample.

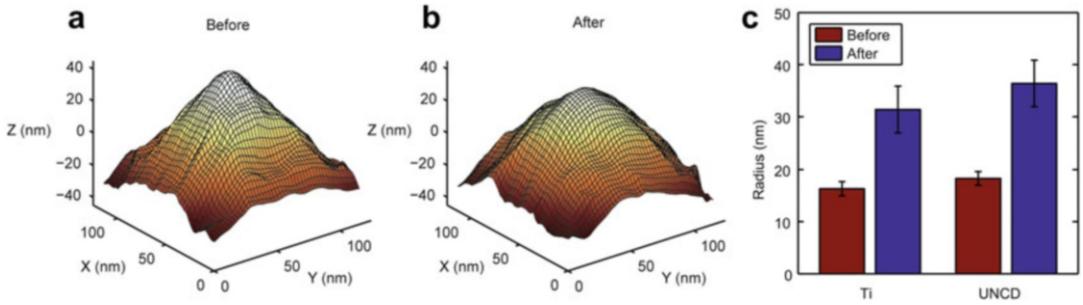

Fig. 3 Results of controlled wear experiments of an AFM tip. Reconstruction of an AFM tip before (**a**) and after (**b**) wear on an ultrananocrystalline diamond. (**c**) Increase in curvature radii of silicon nitride tips by wear experiments on titanium (Ti) and ultrananocrystalline diamond (UNCD) surfaces. Figure reproduced from ref. 21 with permission from Nature Publishing Group.

same chemical properties, but different radii were created. Furthermore, a new method for estimation of tip diameter was presented and compared to the conventionally used blind tip estimation method. In this new approach individual peaks were fit, by using parabolic functions, to the extracted line profiles of the fast scanning axis of AFM images. Figure 3 shows example images of the increase in tip size and a quantification of the increase in tip radii.

We will now take a closer look at the force which acts between the cantilever tip and the sample surface. For this reason, one needs a description of the occurring force while approaching the tip to the surface. A Lennard-Jones potential is suitable to describe the interaction of a surface atom and the tip. In total, the potential is the sum of the interaction of the tip with each surface atom [22]. The expression $U(r) = -\frac{A}{r^6} + \frac{B}{r^{12}}$, where r is the distance between the tip and the sample and $A \approx 10^{-77}$ Jm^6 and $B \approx 10^{-134}$ Jm^{12}, represents the interaction of atoms in a solid [4]. Using the relationship $F(r) = -(\mathrm{d}U/\mathrm{d}r)$, one can calculate the interaction force between the tip and the surface atom. Figure 4 illustrates such a schematic force–distance curve.

Since the force can be attractive ($F < 0$) and repulsive ($F > 0$), there are different regimes that have to be considered. Transferring such a curve on a real AFM system, such a force–distance curve can be acquired by displaying the deflection of the cantilever. Imagine the situation that the cantilever is far away from the sample surface. Here it is unaffected by interactions with the surface and therefore not bent. Approaching the surface, the tip experiences an attractive force. Once the gradient of the attractive force equals the cantilever spring constant the tip jumps into contact with the surface. With further "approach," a force is applied to the surface. According to Newton's third law the sample also exerts the same force on the tip. Thus, the tip is now getting into the repulsive force regime. The force will increase until a certain deflection value, as set by the

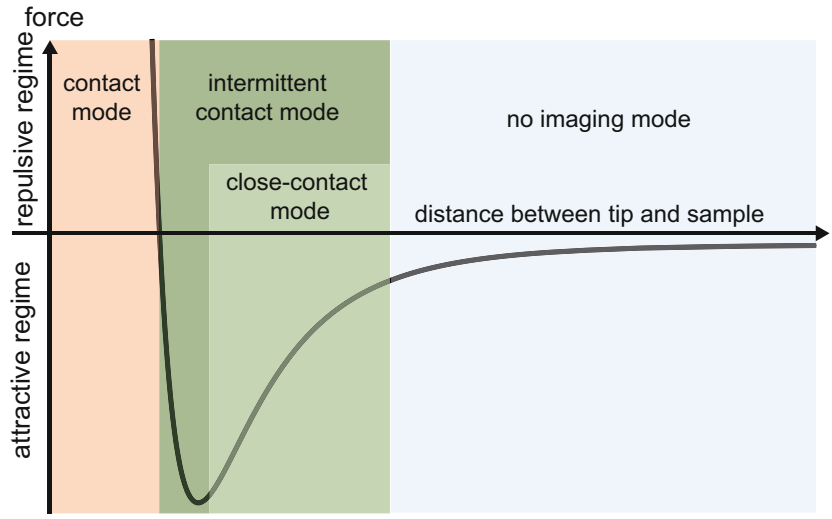

Fig. 4 Schematic illustration of a force–distance curve to illustrate the interaction between the cantilever tip (probe) and the sample surface labeling the different operation modes.

operator, is reached. Reversing the direction of movement, the force is decreased, passing the attractive force regime again, until a jump off occurs. The connection between the tip and the surface is interrupted [4, 5].

2.2 Operation Modes

Having considered the process of approach of the tip towards the sample surface, the various operation modes of AFM can be discussed. By means of Fig. 4, the different force regimes enable a classification of some of these modes. In the following, we will introduce the main modes and their function. In addition, some of their advantages and drawbacks will be discussed.

2.2.1 Contact Mode

The most intuitive operation mode of an AFM is the contact mode. As the name suggests, in this operation mode the tip is continuously in contact with the sample surface. Contact mode operates in the repulsive force regime (Fig. 4) and a force is continuously applied to the surface. In constant force mode, the tip is approached to the surface until a set deflection/force occurs. In this configuration, the surface is scanned while keeping the set force constant with feedback control. The latter implies an "error," meaning the correction voltage that is used to adjust the position of the cantilever. Next to the piezo extension, this "error signal" can also be used to display surface features of the sample. Besides constant force mode, it is also possible to operate in the so-called constant height mode, in which the height of the scanner is fixed. Here, the change in cantilever deflection, and thus the interaction force, is used to directly map the topography of the surface. Consequently, this mode is typically only used for relatively flat surfaces.

An advantage of this operation mode is the high resolution of the obtained images, since there exists a constant contact between the probe and the sample. Another advantage is that it is a fast and straightforward imaging mode. For biological and other soft samples, however, contact mode operation also has some clear disadvantages. Since a force is constantly applied to the surface, chances of sample damage increase. In particular, a constant lateral force arises while scanning, which can drag and slide features over the surface. The result is a distorted image of the sample. It can also happen that the feature of interest is damaged or removed from the surface. In contrast, not only the tip can damage the surface, but also the tip can be damaged by the sample or the scanning process itself, which typically can occur while imaging relatively hard surfaces.

2.2.2 Oscillating Modes

Contact mode imaging is based on the contact between the tip and the surface throughout the whole scan period, which causes large interaction forces with possible destruction of the sample. In order to minimize these forces, there are other operation modes developed based on the oscillation of the cantilever. Such modes are also referred to as dynamic operation modes. In these modes, the cantilever is driven near or at its resonance frequency. The tip touches the surface periodically and during most of the cycle no vertical force is applied to the sample. Furthermore, the lateral forces are markedly reduced during scanning as the major part of the lateral movement occurs when the tip is not in contact with the surface. These two features result in an overall gentler treatment of the sample. Due to the acting force between the surface and the oscillating cantilever when it is approached, the amplitude, the phase as well as the frequency of the oscillation are affected. An integrated feedback control records this change and adapts the piezo element settings if corrections are needed. The choice of the amplitude value can lead to a further distinction of this operation mode class. A variety of different descriptions has been reported and they are partially still under debate. We give a few examples here. If the amplitude that is set is small ($\leq$20 nm [23]), the operation mode is sometimes called "close-contact mode". This mode has also been referred to as "non-contact mode", whereby this term can be misleading, because at least temporarily there exists contact between the probe and the sample. Working in the attractive force regime has the big advantage, that only small interaction forces occur while a high resolution is maintained. To prevent the cantilever from jumping into the repulsive force regime, stiff cantilevers (~40 N/m) are used [24]. When a large amplitude (up to ~100 nm) is set, the corresponding operation mode is called "intermittent contact mode" [24]. Oscillated with a large amplitude, the cantilever passes through the different force regimes, where the interaction force between the probe and the sample can be

repulsive, attractive or even negligible. Consequently, a higher force is applied, which can lead to damage of the sample. On the other hand, the implementation is much easier [5].

2.2.3 Jumping Mode Imaging

Another imaging mode, which has recently gained a lot of attention, measures force vs. distance curves at each pixel and moves the cantilever laterally when the tip is not in contact with the surface. The corresponding operation mode is known under a variety of names, for instance "jumping mode" [25, 26], "Quantitative Imaging (QI^{TM}) mode" [27] or "peak force mode" [28] depending on the manufacturer of the appropriate AFM. As the applied force to the surface is precisely controlled and shear forces are practically absent, this imaging mode allows for controlled measurements on soft, biological samples with possible imaging forces below 100 pN. On each position of the surface a force–distance curve is performed and thereby it does not only give topography information on the sample, but also quantitative mechanical information. Therefore, this imaging mode can be regarded as an extension of traditional "force spectroscopy" AFM. Force spectroscopy is not an AFM imaging mode, but a mode that probes mechanical properties at a certain location at the surface. In particular, the cantilever is pulling or pushing at a set position to exert a force onto the surface. Jumping mode imaging and the related imaging techniques are extending the one-dimensional force spectroscopy to three dimensions to include topography information on the surface. This imaging technique is especially suited to image fragile samples as for instance large protein shells or vesicles.

2.2.4 Operation Environments

AFM imaging can be carried out in liquid, gas or in vacuum. Especially for biological samples the *in-liquid* imaging capability of the technique is of great advantage, because in such a way a near-physiological environment can be obtained. Furthermore, the interfering influences caused by a meniscus of water covering the tip or the sample when imaging in air are eliminated. Fluorescence imaging of biomolecules can relatively easily be combined with AFM in liquid. Working in a liquid environment requires a liquid cell and care must be taken to prevent any harm to the sensitive electronics, in particular the piezo elements. Heating and cooling of the sample is possible under in-liquid conditions, but a decrease in imaging stability is likely the result.

While many biological samples are imaged in liquid [8, 29], in the protein-nucleic acid interaction research field imaging under ambient conditions (i.e. in air) is common practice [30, 31]. For these in air studies it is even possible to combine the imaging with fluorescence microscopy [32]. The fact that the fluorophores still work well under ambient conditions is probably related to the presence of a hydrating water layer on the surface. It is also possible

to operate the AFM in air under controlled temperature conditions. However, it should be considered that heating up the sample can destroy the scanner, while by cooling it down condensation on the sample surface and the optics can occur. An investment in thermal isolation and working in a dry environment is recommended to conduct this kind of experiments.

3 The New Perspective: High-Speed AFM

As the capture of an AFM image takes several minutes, only a snapshot of each line in the sample is obtained and typically only static surfaces are imaged. Still it is possible to study dynamics on surfaces such as AFM-induced changes in biomaterials. Viruses can for instance be moved around by the tip on a surface [33] and AFM tip-induced dissociation of RecA-DNA filaments was performed at a frame rate of 80 s/frame [34]. However, in order to study dynamic biological processes this imaging rate is not sufficient and "real-time" observation is required which is impossible using traditional AFM. This lack of temporal resolution has been a great draw-back of AFM imaging ever since its invention and has effectively prohibited the study of dynamic biological processes. Efforts to achieve a faster scanning rate have been conducted at least since the early 1990s [13]. A high-speed AFM (HS-AFM) approach was reported in 2001, where myosin V conformational changes were studied in real time in liquid. 100×100 pixels^2 images (scan size: 240 nm $\times$ 240 nm) were recorded with a frame rate of 80 ms/frame [35]. Further progress occurred and in 2008 imaging rates of ~40 ms/frame over an area of ~250 nm $\times$ ~250 nm with 100 scan lines were reported [13, 14]. Still at that time this was far from a common approach and only recently HS-AFM is becoming available to a larger group of researchers. How was the increase in imaging rate achieved for HS-AFM? Next to an improvement of the electronics and feedback system, this was done by increasing the resonance frequency of the cantilevers to allow for faster scanning. The resonance frequency could be increased by drastically decreasing the dimensions of the cantilever. Furthermore, the interaction force between the tip and the surface is decreased as well. The latter allows for the investigation of sensitive biological samples. The ratio of the cantilever's resonance frequency and its spring constant affects the sensitivity of the force gradient between the tip and the sample surface. In addition, for the acquisition of high resolution AFM images in dynamic mode in liquid, a balance between the amplitude of the oscillation and the cantilever's stiffness needs to be found. This balance should accommodate a high stability and, simultaneously, an interaction force that facilitates sensitive measurements [13]. To increase the scope of applications in biological sciences, a larger

scan size is desirable. In 2016 Uchihashi *et al.* presented a HS-AFM wide-area scanner which facilitates scanning of an area of ~46 μm × 46 μm. By means of this wide-area scanner a topographic image of *Bacillus subtilis* at 15 s/frame was acquired and bacteriolysis of *B. subtilis* after exposure to lysozyme was observed at 20 s/frame [36]. To position the tip in the right place with this scanner a light microscope was used. The addition of a light microscope has created the possibility of combining HS-AFM with confocal and (super-resolution) fluorescence microscopy. All in all the development of HS-AFM has led to a major increase in temporal resolution thereby opening the door to a wide range of applications including the study of biological processes that occur at time scales of 10s of milliseconds to seconds [15, 37, 38].

4 AFM Applications in Biological Sciences

The field of application of AFM measurements in biological sciences is wide. Not only the imaging of proteins is possible, but also lipid membranes, prokaryotic and eukaryotic cells and nucleic acids can be visualized [1, 5, 29, 39–41] . In addition, AFM can be used to determine the roughness of potential implants including determining the effect of surface treatments of such implants [42–44]. Next to imaging, another broad field of AFM application is force spectroscopy. It does not only give information about adhesion factors [45], but can also be used to study inter- and intramolecular forces including unbinding and unfolding of proteins [7, 46–50]. Such experiments include, as examples, unbinding events in virus-cell interactions and the unfolding of an autotransporter passenger protein [51, 52]. In the former a virus was bound to a cantilever tip and approached to the cell surface to initiate binding, upon which the cantilever was retracted to measure the unbinding events, as shown in Fig. 5a. In the latter, it was revealed how protein secretion through the outer membrane is driven by the folding of the protein into a helical structure which is stabilised by aromatic residues. Figure 5b shows an example unfolding curve, which was used in an inverse approach to reveal the folding and secretion mechanism of this autotransporter protein. In another approach conformational changes related to gating of membrane channels were probed by force spectroscopy [53] (Fig. 5c). Here it was shown that the channel open state exhibits essential differences in mechanical coupling between the transmembrane domains with respect to the closed state.

The above described experiments are “pulling”-type of experiments, but it is also possible to perform “pushing”-type of experiments. This is typically called nano-indentation. During these experiments, the tip is approached to the sample at a fixed position until a set force is reached. This force is typically much larger than

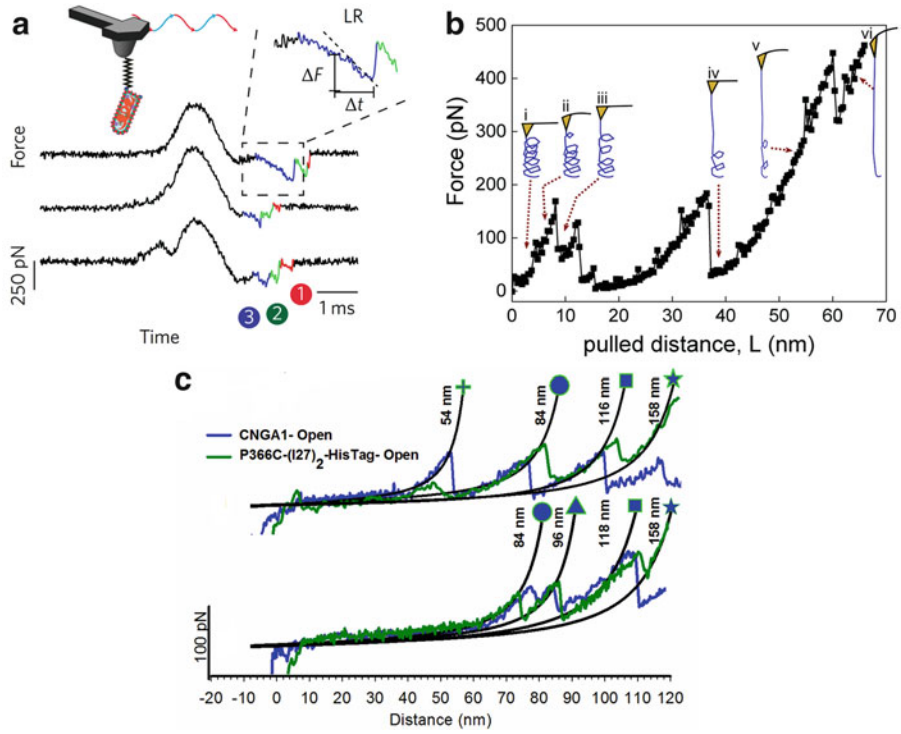

Fig. 5 (**a**) Three virus-cell unbinding event curves in which each curve shows, in color coding, three unbinding events, labeled *1*, *2,* and *3*. Reproduced from ref. 52 with permission from Nature Publishing Group. (**b**) Complete unfolding of an autotransporter protein construct with schematically added figures of the protein at different unfolding stages and the associated cantilever bending (bending is exaggerated for clarity). Reproduced from ref. 51 with permission from American Chemical Society (Copyright 2016). (**c**) Example force curves of unfolding channels in the open state. Worm like chain fits are performed to deduce the increase in contour length during unfolding. Reproduced from ref. 53 with permission from Nature Publishing Group.

the force used for imaging, i.e. it is in the 100s of pN to nN range. Nano-indentation experiments were performed on a variety of particles such as for instance viral protein shells [54–56]. These studies have revealed how viruses possess intriguing mechanical structures [57–59]. We will briefly discuss AFM experiments on the bacteriophage HK97 [57]. This phage self-assembles into an icosahedral procapsid structure, without the dsDNA genome in place. As a next step a maturation step takes place, in which the DNA is packaged with the help of a molecular motor. Concomitantly with this packaging, an increase of the capsid diameter of ~50 nm to ~60 nm occurs. During this expansion, no material is added, so it logically follows that the shell turns thinner. The intriguing question is whether this decrease in thickness is changing the mechanical properties of the protein shell. Nano-indentation experiments were set out to address this question. Figure 6 shows

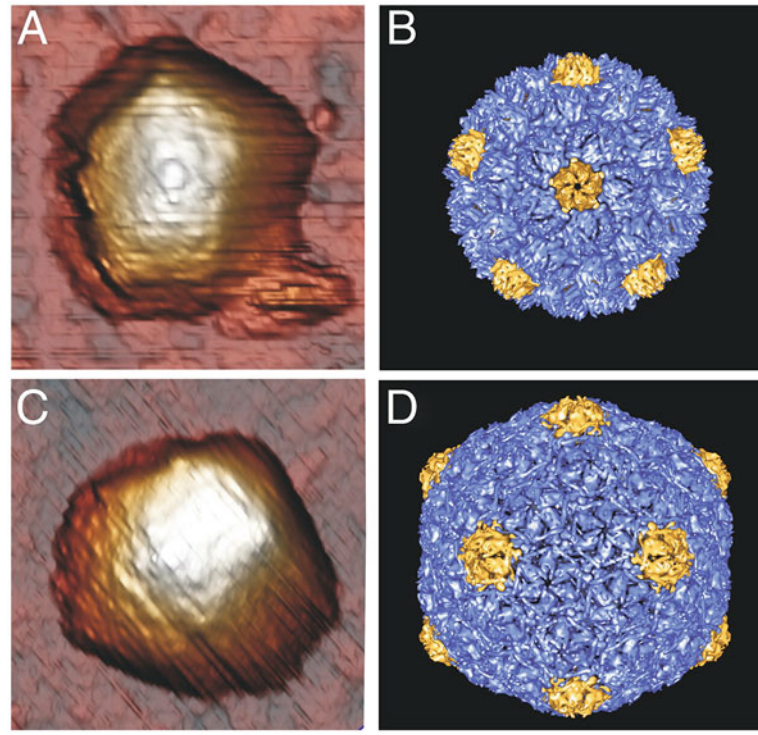

Fig. 6 HK97 procapsid and mature capsid. (**a**, **b**) Respectively AFM image and reconstruction of procapsid lying on its fivefold icosahedral axis. (**c**, **d**) Respectively AFM image and reconstruction of mature capsid lying on its twofold icosahedral axis. Reproduced from ref. 57 with permission from the US National Academy of Sciences.

images of the procapsid and the mature capsid before indentation and for reference the reconstructions of the particles are shown as well. In these images, one can readily differentiate between the icosahedral orientations along which the particles are adsorbed onto the surface. Indentation studies showed a marked difference in material properties between the two types of particles. It turns out that despite its thinner shell, the mature capsid is much stronger than the procapsid. This can only be explained by a detailed scrutinizing of the particle's structure. While the procapsid proteins are loosely attached, during maturation covalent crosslinking occurs between the capsid proteins. This leads to a chainmail like configuration strengthening the particles in an effective manner. These effects are directly related to the bacteriophage infection cycle. During self-assembly the proteins need to be loosely attached, to correct for possible mistakes during assembly. However, after the complete shell has closed, DNA packaging occurs with the help of a molecular packaging motor and considerable forces are exerted

onto the capsid. To be able to withstand these forces a strengthening of the shell is needed and HK97 solved this challenge by adding covalent crosslinks to link the capsid proteins to each other in a solid manner.

5 Conclusion

In this chapter the fundamentals of AFM as well as some of its applications for studying biological samples were presented. This technique can be used for high-resolution three-dimensional imaging at the nanometer scale. Various imaging modes and their suitability to investigate biological samples were discussed. Furthermore, it was shown how force spectroscopy approaches can be used to obtain mechanical information on biological samples, e.g. of protein nanocages and single proteins. Next to traditional AFM, the prospects of high-speed AFM with a focus on biological research fields were indicated. Due to the largely increased imaging speed of this instrument, it is possible to investigate dynamic biological processes on the ms time scale. For instance the movement of myosin V could be observed in real-time [37]. Consequently, AFM is shown to be a versatile technique in biological sciences to obtain morphological and mechanical information on proteins, proteinaceous assemblies, membranes, and nucleic acids. Furthermore, by using high-speed AFM also dynamic processes can be studied. With the advent of new, gentle imaging techniques and fast scanning approaches it is expected that the use and applicability of AFM in life sciences will become even more relevant in the time to come.

Acknowledgement

This work is supported by the STW Perspectief grant CANCER-ID and a Nederlandse Organisatie der Wetenschappen Vidi vernieuwingsimpuls grant (both to WHR).

References

1. Demtröder W (ed) (2010) Experimentalphysik 3, Kern-, Teilchen- und Astrophysik, 4th edn. Springer, Berlin
2. Binnig G, Rohrer H, Gerber C, Weibel E (1982) Surface studies by scanning tunneling microscopy. Phys Rev Lett 49:57–61
3. Binnig G, Quate CF (1986) Atomic force microscope. Phys Rev Lett 56:930–933
4. de Pablo PJ (2011) Introduction to atomic force microscopy. Meth Mol Biol 783:197–212
5. Eaton P, West P (eds) (2010) Atomic force microscopy. Oxford Univesity Press, Oxford
6. Kodera N, Ando T (2014) The path to visualization of walking myosin V by high-speed atomic force microscopy. Biophys Rev 6:237–260
7. Santos NC, Castanho MARB (2004) An overview of the biophysical applications of atomic force microscopy. Biophys Chem 107:133–149

8. Baclayon M, Wuite GJL, Roos WH (2010) Imaging and manipulation of single viruses by atomic force microscopy. Soft Matter 6:5273–5285
9. Marchetti M, Wuite GJL, Roos WH (2016) Atomic force microscopy observation and characterization of single virions and virus-like particles by nano-indentation. Curr Opin Virol 18:82–88
10. Morris VJ, Kirby AR, Gunning AP (eds) (2009) Atomic force microscopy for biologists, 2nd edn. London, Imperial College Press
11. Gross R, Marx A (eds) (2012) Festkörperphysik, 1st edn. München, Oldenbourg Verlag
12. Ando T (2012) High-speed atomic force microscopy coming of age. Nanotechnology 23:062001
13. Ando T, Uchihashi T, Fukuma T (2008) High-speed atomic force microscopy for nano-visualization of dynamic biomolecular processes. Prog Surf Sci 83:337–437
14. Ando T, Uchihashi T, Kodera N *et al.* (2008) High-speed AFM and nano-visualization of biomolecular processes. Pflügers Arch Eur J Physiol 456:211–225
15. Eghiaian F, Rico F, Colom A *et al.* (2014) High-speed atomic force microscopy: Imaging and force spectroscopy. FEBS Lett 588:3631–3638
16. Rugar D, Hansma P (1990) Atomic force microscopy. Phys Today 43:23–30
17. Roos WH, Radtke K, Kniesmeijer E *et al.* (2009) Scaffold expulsion and genome packaging trigger stabilization of herpes simplex virus capsids. Proc Natl Acad Sci USA 106:9673–9678
18. Meyer G, Amer NM (1988) Novel optical approach to atomic force microscopy. Appl Phys Lett 53:1045
19. Churnside AB, Sullan RMA, Nguyen DM *et al.* (2012) Routine and timely sub-picoNewton force stability and precision for biological applications of atomic force microscopy. Nano Lett 12:3557–3561
20. Sader JE, Chon JWM, Mulvaney P (1999) Calibration of rectangular atomic force microscope cantilevers. Rev Sci Instrum 70:3967–3969
21. Vorselen D, Kooreman ES, Wuite GJL, Roos WH (2016) Controlled tip wear on high roughness surfaces yields gradual broadening and rounding of cantilever tips. Sci Rep 6:36972
22. Hölscher H, Allers W, Schwarz UD *et al.* (2000) Interpretation of "true atomic resolution" images of graphite (0001) in noncontact atomic force microscopy. Phys Rev B 62:6967
23. Ho H, West P (1996) Optimizing AC-mode atomic force microscope imaging. J. Scan Microsc 18:339–343
24. García R, Pérez R (2002) Dynamic atomic force microscopy methods. Surf Sci Rep 47:197–301
25. de Pablo PJ, Colchero J, Gómez-Herrero J, Baró AM (1998) Jumping mode scanning force microscopy. Appl Phys Lett 73:3300
26. Moreno-Herrero F, Colchero J, Gómez-Herrero J, Baro AM (2004) Atomic force microscopy contact, tapping, and jumping modes for imaging biological samples in liquids. Phys Rev E 69:1–9
27. JPK Instruments (2011) Nanowizard 4 – the next benchmark for BioAFM. JPK Instruments, Berlin
28. Bruker Nano Surfaces Division (2015) PeakForce tapping – how AFM should be. Bruker Nano Surfaces Division, Goleta, CA
29. Engel A, Müller DJ (2000) Observing single biomolecules at work with the atomic force microscope. Nat Struct Biol 7:715–718
30. Bustamante C, Rivetti C (1996) Visualizing protein-nucleic acid interactions on a large scale with the scanning force microscope. Annu Rev Biophys Biomol Struct 25:395–429
31. Farge G, Mehmedovic M, Baclayon M *et al.* (2014) In vitro-reconstituted nucleoids can block mitochondrial DNA replication and transcription. Cell Rep 8:66–74
32. Sanchez H, Kanaar R, Wyman C (2010) Molecular recognition of DNA–protein complexes: a straightforward method combining scanning force and fluorescence microscopy. Ultramicroscopy 110:844–851
33. Falvo MR, Washburn S, Superfine R *et al.* (1997) Manipulation of individual viruses: friction and mechanical properties. Biophys J 72:1396–1403
34. van der Heijden T, Moreno-Herrero F, Kanaar R *et al.* (2007) Comment on "Direct and Real-Time Visualization of the Disassembly of Single RecA-DNA-ATP(gamma)S Complex" using AFM imaging in fluid. Nano Lett 6:3000–3002
35. Ando T, Kodera N, Takai E *et al.* (2001) A high-speed atomic force microscope for studying biological macromolecules. Proc Natl Acad Sci U S A 98:12468–12472
36. Uchihashi T, Watanabe H, Fukuda S *et al.* (2016) Functional extension of high-speed AFM for wider biological applications. Ultramicroscopy 160:182–196
37. Kodera N, Yamamoto D, Ishikawa R, Ando T (2010) Video imaging of walking myosin V by

high-speed atomic force microscopy. Nature 468:72–76

38. Nievergelt AP, Erickson BW, Hosseini N *et al.* (2015) Studying biological membranes with extended range high-speed atomic force microscopy. Sci Rep 5:11987
39. Henderson E (1992) Imaging and nano dissection of individual supercoiledplasmids by atomic force microscopy. Nucleic Acids Res 20:445–447
40. Baclayon M, Roos WH, Wuite GJL (2010) Sampling protein form and function with the atomic force microscope. Mol Cell Proteomics 9:1678–1688
41. Lekka M (2016) Discrimination between normal and cancerous cells using AFM. Bionanoscience 6:65–80
42. Lamolle SF, Monjo M, Lyngstadaas SP *et al.* (2009) Titanium implant surface modification by cathodic reduction in hydrofluoric acid: Surface characterization and in vivo performance. J Biomed Mater Res A 88:581–588
43. Larsson Wexell C, Thomsen P, AronssonB-O*et al.* (2013) Bone response tosurface-modifiedtitanium implants: studies on the early tissue response to implants with different surface characteristics. Int J Biomater 2013:1–10
44. Kroeze RJ, Helder MN, Roos WH *et al.* (2010) The effect of ethylene oxide, glow discharge and electron beam on the surface characteristics of poly(L-lactide-co-caprolactone) and the corresponding cellular response of adipose stem cells. Acta Biomater 6:2060–2065
45. de Pablo PJ, Colchero J,Gomez-HerreroJ *et al.* (1999) Adhesion maps using scanning force microscopy techniques. J Adhes 71:339–356
46. Mitsui K, Hara M, Ikai A (1996) Mechanical unfolding of α_2-macroglobulinatomic force microscope. FEBS Lett 385:29–33
47. Rief M, Gautel M, Oesterhelt F *et al.* (1997) Reversible unfolging of individual titin immunoglobulin domains by AFM. Science 276:1109–1112
48. Hinterdorfer P, Dufrêne YF (2006) Detection and localization of single molecular recognition events using atomic force microscopy. Nat Methods 3:347–355
49. Kasas S, Thomson NH, Smith BL *et al.* (1997) Escherichia coli RNA polymerase activity observed using atomic force microscopy. Biochemistry 36:461–468
50. Kasas S, Dietler G (2008) Probing nanomechanical properties from biomolecules to living cells. Pflügers Arch Eur J Physiol 456:13–27
51. Baclayon M, van Ulsen P, Mouhib H *et al.* (2016) Mechanical unfolding of an autotransporter passenger protein reveals the secretion starting point and processive transport intermediates. ACS Nano 10:5710–5719
52. Alsteens D, Newton R, Schubert R *et al.* (2016) Nanomechanical mapping of first binding steps of a virus to animal cells. Nat Nanotechnol 12(2):177–183. doi: 10.1038/nnano.2016.228
53. Maity S, Mazzolini M, Arcangeletti M *et al.* (2015) Conformational rearrangements in the transmembrane domain of CNGA1 channels revealed bysingle-moleculeforce spectroscopy. Nat Commun 6:7093
54. van Rosmalen MGM, Roos WH, Wuite GJL (2015) Material properties of viral nanocages explored by atomic force microscopy. Meth Mol Biol 1252:115–137
55. Roos WH, Wuite GJL (2009) Nanoindentation studies reveal material properties of viruses. Adv Mater 21:1187–1192
56. Mateu MG (2012) Mechanical properties of viruses analyzed by atomic force microscopy: a virological perspective. Virus Res 168:1–22
57. Roos WH, Gertsman I, May ER *et al.* (2012) Mechanics of bacteriophage maturation. Proc Natl Acad Sci U S A 109:2342–2347
58. Carrasco C, Luque A, Hernando-Pérez M *et al.* (2011)Built-inmechanical stress in viral shells. Biophys J 100:1100–1108
59. Baclayon M, Shoemaker GK, Uetrecht C *et al.* (2011) Prestress strengthens the shell of Norwalk virus nanoparticles. Nano Lett 11:4865–4869